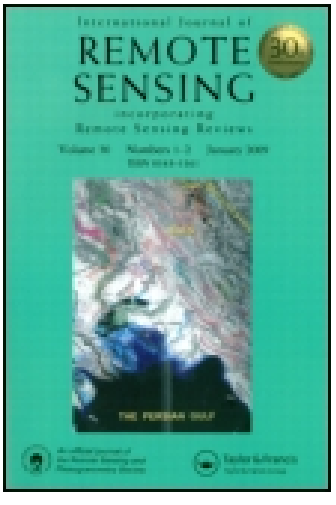

International Journal of Remote Sensing

Publication details, including instructions for authors and subscription information:
http://www.tandfonline.com/loi/tres20

Performance of atmospheric and topographic correction methods on Landsat imagery in mountain areas

Steven Vanonckelen[a], Stef Lhermitte[b], Vincent Balthazar[c] & Anton Van Rompaey[a]

[a] Division of Geography, Katholieke Universiteit Leuven, BE-3001 Heverlee, Belgium

[b] Royal Netherlands Meteorological Institute, AE-3730 De Bilt, The Netherlands

[c] Earth and Life Institute, Université Catholique de Louvain, BE-1348 Louvain-La-Neuve, Belgium

Published online: 25 Jul 2014.

To cite this article: Steven Vanonckelen, Stef Lhermitte, Vincent Balthazar & Anton Van Rompaey (2014) Performance of atmospheric and topographic correction methods on Landsat imagery in mountain areas, International Journal of Remote Sensing, 35:13, 4952-4972

To link to this article: http://dx.doi.org/10.1080/01431161.2014.933280

International Journal of Remote Sensing, 2014
Vol. 35, No. 13, 4952–4972, http://dx.doi.org/10.1080/01431161.2014.933280

Performance of atmospheric and topographic correction methods on Landsat imagery in mountain areas

Steven Vanonckelen[a]*, Stef Lhermitte[b], Vincent Balthazar[c], and Anton Van Rompaey[a]

[a]*Division of Geography, Katholieke Universiteit Leuven, BE-3001 Heverlee, Belgium;* [b]*Royal Netherlands Meteorological Institute, AE-3730 De Bilt, The Netherlands;* [c]*Earth and Life Institute, Université Catholique de Louvain, BE-1348 Louvain-La-Neuve, Belgium*

(*Received 1 August 2013; accepted 20 March 2014*)

An effective removal of atmospheric and topographic effects on remote-sensing imagery is an essential preprocessing step for mapping land cover accurately in mountain areas. Various techniques that remove these effects have been proposed and consist of specific combinations of an atmospheric and a topographic correction (TC) method. However, it is possible to generate a wide range of new combined correction methods by applying alternative combinations of atmospheric and TC methods. At present, a systematic overview of the statistical performance and data input requirement of preprocessing techniques is missing. In order to assess the individual and combined impacts of atmospheric and TC methods, 15 permutations of two atmospheric and/or four TC methods were evaluated statistically and compared to the uncorrected imagery. Furthermore, results of the integrated ATCOR3 method were included. This evaluation was performed in a study area in the Romanian Carpathian mountains. Results showed that the combination of a transmittance-based atmospheric correction (AC), which corrects the effects of Rayleigh scattering and water-vapour absorption, and a pixel-based C or Minnaert TC, which account for diffuse sky irradiance, reduced the image distortions most efficiently. Overall results indicated that TC had a larger impact than AC and there was a trade-off between the statistical performance of preprocessing techniques and their data requirement. However, the normalized difference vegetation index analysis indicated that atmospheric methods resulted in a larger impact on the spectral information in bands 3 and 4.

1. Introduction

Worldwide, mountain areas are experiencing rapid land-cover changes that affect a set of ecosystem services, such as soil and water conservation, biodiversity preservation, and carbon sequestration (Defries, Foley, and Asner 2004; Foley et al. 2005; Lambin and Meyfroidt 2010; World Health Organization 2005). Not surprisingly, increasing efforts are invested in land-cover monitoring and mapping of mountain areas. The relative inaccessibility of mountain areas favours remote-sensing techniques as a monitoring tool (Lambin and Geist 2006; Turner, Lambin, and Reenberg 2007). Implementation of remote-sensing tools is, however, often hampered by problems originating from atmospheric and topographic distortions (Singh, Sharma, and Mishra 2011). Therefore, preprocessing techniques are an essential step to improve interpretation of satellite imagery.

Atmospheric correction (AC) methods aim at removing distortions caused by the interaction between radiance and atmosphere (e.g. molecular scattering and absorption by gases). The most popular AC method is the dark object subtraction method (Chavez

*Corresponding author. Email: steven.vanonckelen@ees.kuleuven.be

1996). A list of more advanced radiative transference models is provided in Table 1. Some AC methods are based on transmittance functions (TFs): the moderate spectral resolution atmospheric transmittance algorithm (Berk et al. 1998), the atmospheric part of the integrated radiometric correction method by Kobayashi and Sanga-Ngoie (2008), and the atmospheric part of the ATCOR3 method (Richter 1996, 1998). These last two ACs are explained in the Section 3. Topographic correction (TC) aims at removing topographic distortions by deriving the radiance that would be observed in a flat terrain. A list of TCs is shown in Table 1. Three major types of TC methods have been developed. The simplest of these methods involves empirical normalizations, such as spectral band ratioing (Colby 1991; Ono, Kajiwara, and Honda 2007). Geometrical corrections assuming Lambertian reflection are considerably more sophisticated, such as cosine correction (Teillet, Guindon, and Goodenough 1982). Most advanced geometrical corrections assume non-Lambertian behaviour, such as Minnaert corrections (Bishop and Colby 2002; Lu et al. 2008; Minnaert 1941; Smith, Lin, and Ranson 1980), C-correction (Teillet, Guindon, and Goodenough 1982) and sun–canopy–sensor correction. For example, Minnaert correction can be used over a flat terrain only to normalize the observations to a nadir geometry, and in mountain areas to correct topographic distortions (Johnson, Peddle, and Hall 2000).

During the past 30 years, AC and TC methods have mainly been evaluated individually, which is shown in Table 1. As tested by Schroeder et al. (2006) and Vicente-Serrano, Perezcabello, and Lasanta (2008), the major distortions in Landsat bands 4 to 7 originated from differential illumination due to topography, since longer wavelengths were less susceptible to aerosol effects. The C-correction reduced differences between north- and south-facing slope reflectances of Landsat imagery, especially in bands 3 and 4 (Vicente-Serrano, Perezcabello, and Lasanta 2008). So far, only a limited number of AC and TC combinations have been tested, which are shown in Table 1. Differences in spectral values were reduced for similar land-cover types, and spectral properties became more homogeneous for different illumination angles. A maximum of five individual AC and/or TC methods have been implemented and compared by Riano et al. (2003) and Vicente-Serrano, Perezcabello, and Lasanta (2008). The analysis of Riano et al. (2003) compared one AC and four TCs, while Vicente-Serrano, Perezcabello, and Lasanta (2008) compared effects of two AC and two TC methods in 2008. In principle, many more 'new' integrated or combined models can be built with individual AC and TC methods. Appropriate combined corrections are selected according to the study area, available data, and implementation time. Furthermore, the influence of integrated AC and TC methods has been evaluated. Examples are the IRC method of Kobayashi and Sanga-Ngoie (2008) and the ATCOR3 method of Richter (1996, 1998). Kobayashi and Sanga-Ngoie (2008) showed that an integrated correction resulted in nearly flat regression lines between $\cos \beta$ (β is the incident solar angle) and corrected radiances. A major disadvantage of integrated corrections is the implementation of a specific AC and TC, as shown in Table 1. Existing preprocessing techniques are based on a specific combination of an atmospheric and a TC and many more combinations that are described in the literature are possible. In order to select the most appropriate preprocessing steps, the performance of combined corrections should be evaluated based on different individual AC and TC components.

The added value of this study is the decomposition of integrated models in an AC and a TC component. The study is unique since most similar studies to date lack a thorough comparison between different AC and TC methods. However, in order to test for effects of non-linearity, the impact of combined corrections is also compared. Therefore, this article systematically evaluates the effects of all possible combinations of two AC and four TC methods, along with uncorrected imagery. Thereby, a variety of representative methods is

Table 1. Type, correction, reference, and acronym of AC, TC, and integrated (int.) or combined (comb.) methods.

Type	Correction	References	Acronym
AC	LOWTRAN-7	Kneizys et al. (1988)	Low-resolution atmospheric transmission
	RTCs, image-based procedures and DOS	Moran et al. (1992)	Radiative transfer codes
	Inverse technique	Gilabert, Conese, and Maselli (1994)	
	DOS	Chavez (1996)	Dark object subtraction method
	ATCOR2	Richter (1996)	An acronym for atmospheric correction
	SMAC	Rahman and Dedieu (1994)	Simplified method for AC
	6S	Sriwongsitanon, Surakit, and Thianpopirug (2011), Vermote et al. (1997), and Zhao, Tamura, and Takahashi (2001)	Second simulation of a satellite signal in the solar spectrum
	Empirical line	Smith and Milton (1999)	
	AC with look-up tables	Liang, Fang, and Chen (2001) and Liang and Fang (2004)	Dense dark vegetation, modified DDV, and path radiance approach
	DDV, MDDV, and PARA	Song et al. (2001)	This method is the AC part of the integrated radiometric correction
	Transmittance functions (TF)	Kobayashi and Sanga-Ngoie (2008)	
TC	Minnaert	Bishop and Colby (2002), Lu et al. (2008), Minnaert (1941), and Smith, Lin, and Ranson (1980)	
	Band ratios	Colby (1991) and Ono, Kajiwara, and Honda (2007)	
	Cosine	Teillet, Guindon, and Goodenough (1982)	
	Hay's model	Hay (1979)	
	C	Bishop, Shroder, and Colby (2003), Jensen (1996), Meyer et al. (1993), and Teillet, Guindon, and Goodenough (1982)	
	Two-stage topographic normalization	Civco (1989)	
	Minnaert with changing constant and correction based on empirical function SCS	Ekstrand (1996)	Sun–canopy–sensor topographic correction
	Cosine, empiric–statistic, C, and Minnaert correction	Gu and Gillespie (1998) Johnson, Peddle, and Hall (2000)	
	Band ratio, Minnaert, aspect partitioning, and combinations of these corrections	Hale and Rock (2003)	
	C-Huang Wei	Huang et al. (2008)	
	PBC and PBM	Kobayashi and Sanga-Ngoie (2008)	Pixel-based Minnaert and pixel-based C-correction

(*Continued*)

Table 1. (*Continued*).

Type	Correction	References	Acronym
	Empirical line, cosine, C, Minnaert, statistical-empirical, SCS, *b*, SCS + C, and MFM-TOPO	Soenen et al. (2008)	MFM-TOPO is canopy reflectance model-based TC
	Empirical, cosine, C, and Minnaert	Wu et al. (2008)	
	SCS	Huang et al. (2008)	
	Cosine, SCS, *b*, and VECA	Gao and Zhang (2009)	Variable empirical coefficient algorithm
	C, modified Minnaert, and Gamma	Richter, Kellenberger, and Kaufmann (2009)	
	Simplified normalization	Cuo, Vogler, and Fox (2010)	
	Cosine, C, Minnaert, modified Minnaert, and empiric–statistic correction	Hantson and Chuvieco (2011)	
	Cosine, C, smooth C, SCS + C, C-Huang Wei, and slope matching	Singh, Sharma, and Mishra (2011)	
	Modified C-correction	Veraverbeke et al. (2011)	
	Three-factor + C	Zhang and Gao (2011)	
	Cosine, Minnaert, C, SCS, two-stage topo normalization, and slope matching	Zhang et al. (2011)	
Int. or comb.	Inverse technique + band ratios	Conese et al. (1993)	
	ATCOR2 + DEM [ATCOR3]	Richter (1997) and Richter and Schäpfler (2002, 2011)	
	6 S + DEM	Sandmeier and Itten (1997)	
	DOS + Minnaert, C and variation of C	Riano et al. (2003)	
	DOS + cosine and SCS	Vincini and Frazzi (2003)	
	ATCOR2 + Minnaert	Mitri and Gitas (2004)	
	LOWTRAN-7 + Minnaert	Gitas and Devereux (2006)	Integrated radiometric correction
	TF + PBC [IRC]	Kobayashi and Sanga-Ngoie (2008)	
	DTA and 6 S + cosine and C	Vicente-Serrano, Perezcabello, and Lasanta (2008)	Dark target approach
	SIERRA	Lenot, Achard, and Poutier (2009)	Spectral reflectance image extraction from radiance with relief and atmospheric correction
	DOS + Minnaert and SCS	Gao and Zhang (2009)	
	Parameterized BRDF	Wen et al. (2009)	Bidirectional reflectance distribution function

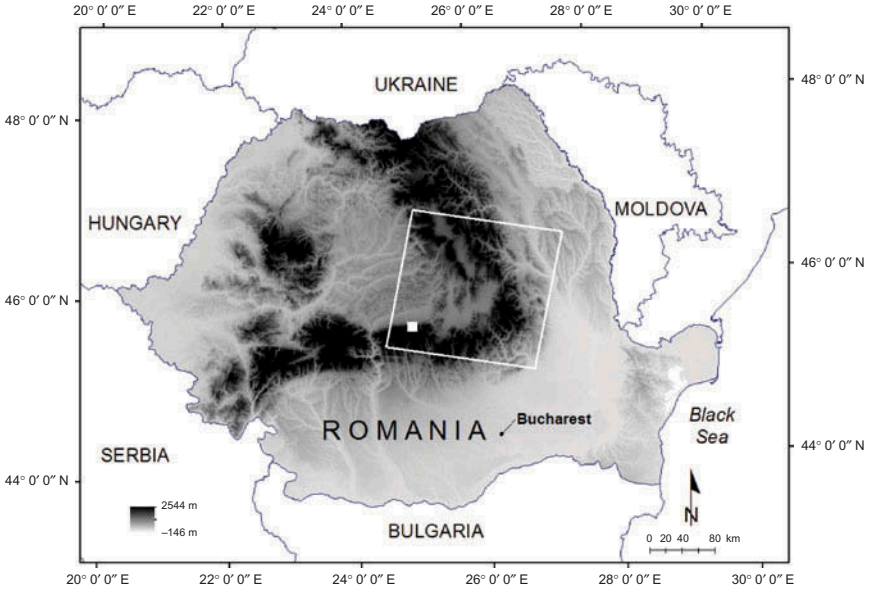

Figure 1. SRTM from Romania and indication of the surrounding countries. The white-outlined rectangle delineates the study area, the solid white rectangle a zoom in the study area.

selected based on their data input requirement and automation complexity. Since ATCOR3 is a popular integrated model, the evaluation of this model is also included in the analyses.

2. Study area and data set

The study area consists of a Landsat-5 Thematic Mapper (TM) image (path 183/row 28) located in the central-eastern Carpathian mountains in Romania (Figure 1). The study area covers 31,110 km^2 and comprises parts of the eastern Carpathian mountains and the Transylvanian Plateau. Elevation ranges between 53 and 2545 m with a mean elevation of 570 m.

The area is characterized by a temperate mountain climate with an average yearly rainfall volume of about 635 mm and a mean annual temperature of about 11°C in central Transylvania. The ridges of the eastern Carpathians consist of crystalline schist and sedimentary and volcanic rock. The steep hillslopes are covered with mixed forests consisting of coniferous (e.g. *Abies alba* and *Picea abies*) and broadleaved trees (e.g. *Betula pendula*, *Carpinus betulus*, and *Fagus sylvatica*) (Kuemmerle et al. 2009). Footslopes and plateaus are used for farming and cattle herding. Total population in the study area is estimated at 2,667,000 people, of which 277,000 live in Brasov and 175,500 in Bacau (NIS Romania 2010). The majority of the population receives an income from farming practices.

The Landsat-5 image from 24 July 2009 was obtained from the archive of the United States Geological Survey. In this analysis, all corrections were performed on six non-thermal bands: three visible bands (0.45–0.52, 0.52–0.60, and 0.63–0.69 μm) and three infrared bands (0.76–0.90, 1.55–1.75, and 2.08–2.35 μm). The image was orthorectified with precision terrain correction level L1T by the United States Geological Survey, and no cloud masking was performed, since cloud coverage in the study area was below 1%. The

solar elevation and azimuth angles were 57.8° and 136.9°, respectively. The digital elevation model (DEM) was the space shuttle radar topography mission (SRTM) from CGIARCSI/NASA, which was co-registered with the Landsat image using automatic tie matching and considering both Landsat displacement and acquisition geometry (root mean square error < 0.5; Leica Geosystems 2006). The SRTM provided a high-quality DEM at resolution levels of 1 arc-second (30 m × 30 m) in the USA or 3 arc-seconds (90 m × 90 m) worldwide (Rabus et al. 2003). Although the ASTER GDEM from the METI/NASA was characterized by a worldwide 1 arc-second resolution, several analyses have indicated that the ASTER GDEM was more subject to artefacts such as stripes or cloud anomalies (Hirt, Filmer, and Featherstone 2010; Van Ede 2004). Therefore, the SRTM version 4.1 was resampled to a pixel size of 30 m × 30 m by means of a bicubic spline interpolation to match the resolution of the Landsat image.

3. Methodology

First, digital numbers of each spectral band were converted into at-sensor radiances ($L_{s,\lambda}$) based on gain and offset values included in the metadata (Chander, Markham, and Helder 2009). Afterwards, at-sensor radiances were not atmospherically corrected or corrected with one of the ACs described below, and converted to at-surface reflectances with Equation (1) (Chander, Markham, and Helder 2009):

$$\rho_{T,\lambda} = \frac{\pi L_{s,\lambda}\, d^2}{(\mathrm{ESUN})_\lambda \cos\theta_s}, \tag{1}$$

where $\rho_{T,\lambda}$ = observed surface reflectance on an inclined surface (dimensionless or %); λ = band wavelength; $L_{s,\lambda}$ = at-sensor radiance (W m^{-2} sr μm); d = earth–sun distance (astronomical units); ESUN_λ = mean exo-atmospheric solar irradiance (W m^{-2} μm); and θ_s = solar zenith angle (°). Furthermore, the ATCOR3 method was applied, which integrates an atmospheric and a TC. In a final step, the normalized reflectances of a horizontal surface ($\rho_{H,\lambda}$) were calculated based on one of the four TC methods described below.

3.1. *Atmospheric corrections*

In this article, a simplified AC, a transmittance-based AC, and no correction were compared on one Landsat scene. Table 2 provides the implemented equations of the AC methods. The first and simplified AC method is the DOS correction, which assumes that observed radiances from dark objects are a good assessment for atmospheric scattering and diffusion. Thereby, a uniform atmosphere across the image is assumed, and DOS only considers the effect of scattering (Bruce and Hilbert 2004). The at-sensor radiance was estimated by subtracting a minimum radiance value ($L_{\min}$) from each pixel, as shown in Equation (2) of Table 2 (Song et al. 2001). The minimum value was calculated for each band as the first percentile radiance value over the entire image and accounts for the atmospheric effect (Chavez 1996).

The second method is the TF AC, which implements the atmospheric part of the IRC method of Kobayashi and Sanga-Ngoie (2008). This correction removes the effects of Rayleigh scattering and water-vapour absorption. TF correction extends the DOS method with a denominator containing normalized and band-specific TFs of water-vapour

Table 2. Equations and references of the two applied atmospheric corrections.

AC	Equations	References
DOS	$L_{p,\lambda} = L_{s,\lambda} - L_{min}$ (2)	Chavez (1996)
TF	$Lp,\lambda = \frac{L_{s,\lambda} - L_{min}}{0.5(1 + T_{r,\lambda})T_{r,\lambda}T_{w,\lambda}^2}$ (3)	Kobayashi and Sanga-Ngoie (2008)
	$T_{r,\lambda} = \exp\left[-\frac{P}{P_0}M\frac{1}{115.6406\lambda^4 - 1.335\lambda^2}\right]$ (4)	
	$M = \frac{1}{\cos\theta_s + 0.15(93.885 - \theta_s)^{-1.253}}$ (5)	
	$T_{w,\lambda} = \exp\left[-\frac{0.2385a_wWM}{(1 + 20.07a_wWM)^{0.45}}\right]$ (6)	

Notes: DOS is the dark object subtraction method, and TF is the AC based on TFs. $L_{p,\lambda}$ (in W m^{-2} sr μm) is the path radiance of the image, and $L_{s,\lambda}$ is the uncorrected radiance of the image. L_{min} represents the minimum radiance value of the image, calculated as the first percentile. $T_{r,\lambda}$ is the Rayleigh scattering TF, including sea-level atmospheric pressure (P_0; in mbar), ambient atmospheric pressure (P; in mbar), and band wavelength (λ). M is the relative air mass, and θ_s is the solar zenith angle (in °). $T_{w,\lambda}$ is the water-vapour TF, calculated with the precipitable water vapour (W; in cm), relative air mass (M), and water-vapour absorption coefficients (a_w).

absorption and Rayleigh scattering, as shown in Equation (3) of Table 2. TFs were calculated for each wavelength and normalized per band. Here, a simplified approach was implemented, calculating the normalized TF for each band based on the mean wavelength. The Rayleigh scattering TF ($T_{r,\lambda}$) was calculated with Equation (4) of Table 2, which is based on sea-level atmospheric pressure (P_0; in mbar), ambient atmospheric pressure (P; in mbar), and wavelength (λ). The value of sea-level atmospheric pressure was assumed to be 1013 mbar, and ambient atmospheric pressure (995 mbar) was obtained from daily mean surface pressures in NASA's atmospheric Giovanni Portal (2012). Relative air mass M was calculated from Equation (5) in Table 2. This value was constant across the study area, since M was only dependent on the solar zenith angle (θ_s). The water-vapour TF ($T_{w,\lambda}$) was calculated from Equation (6) in Table 2 based on the following parameters: precipitable water vapour (W; in cm), relative air mass (M), and water-vapour absorption coefficient (a_w) given as a function of wavelength (Bird and Riordan 1986). The precipitable water vapour (1.39 cm) was obtained from the Aqua satellite in NASA's atmospheric Giovanni Portal (2012) and based on the central point in the image at acquisition. Values of W and P were selected from the centre of the image and were assumed to be constant across the study area. Therefore, central values were compared with values in the four corners of the image. The minima and maxima of these values were only varying from 1% to 5% of the central value.

3.2. *Topographic corrections*

Four different TCs were evaluated in this analysis. Table 3 provides the implemented equations of all TC methods. The first method, band ratioing, is based on the assumption that reflectance values vary proportionally in all bands. The observed reflectance on an inclined terrain ($\rho_{T,\lambda}$) was obtained by calculating the arithmetic mean of observed reflectances over all spectral bands, as shown in Equation (7) of Table 3.

Table 3. Equations and references of the four applied topographic corrections.

TC	Equations	References
Band ratio	$\rho_{H,\lambda}^{(i)} = \frac{\rho_{T,\lambda}^{(i)}}{\frac{1}{N}\sum_{j=1}^{N}\rho_{T,\lambda}^{(j)}}$ (7)	Ono, Kajiwara, and Honda (2007)
Cosine	$\rho_{H,\lambda} = \rho_{T,\lambda}\frac{\cos\theta_s}{\cos\beta}$ (8)	Teillet, Guindon, and Goodenough (1982)
PBM	$\rho_{H,\lambda} = \rho_{T,\lambda}\frac{\cos\theta_n}{(\cos\theta_n\ \cos\beta)^{k,\lambda}}$ (9)	Lu et al. (2008)
PBC	$\rho_{H,\lambda} = \rho_{T,\lambda}\frac{\cos\theta_s + C_\lambda h_0^{-1}}{\cos\beta + C_\lambda h_0^{-1}h}$ (10)	Kobayashi and Sanga-Ngoie (2008)

Notes: PBM is the pixel-based Minnaert correction, and PBC is the pixel-based C-correction. $\rho_{H,\lambda}$ (dimensionless or %) stands for the normalized reflectance of a horizontal surface for a specific spectral band number (N), and $\rho_{T,\lambda}$ stands for the observed reflectance on an inclined terrain. θ_s is the solar zenith angle, and β is the incident solar angle. θ_n is the slope angle of the terrain, and k_λ is the slope of the regression between $x = \log_{10}(\cos\theta_n \cos\beta)$ and $y = \log_{10}(\rho_{T,\lambda}\cos\theta_n)$. Parameter C_λ is the quotient of intercept (b_λ) and slope (m_λ) of the regression line between x and y. The h-factor represents a topographic parameter derived from the SRTM ($h = 1–\theta_n/\pi$), and the h_0-factor represents an empirical parameter derived from the regression line between reflectance and cos β ($h_0 = (\pi + 2\theta_s)/2\pi$).

The second method, cosine correction, assumes a uniform reflectance of incident solar energy in all directions (Lu et al. 2008). The incident solar angle β is the angle between the normal to the ground surface and the solar zenith direction (Civco 1989). The cosine of the incident solar angle was calculated from Equation (11) and varies between −1 and +1:

$$\cos\beta = \cos\theta_s\cos\theta_n + \sin\theta_s\sin\theta_n\cos(\phi_t - \phi_a), \tag{11}$$

where θ_n, ϕ_t, and ϕ_a are the slope angle of the terrain, aspect angle of the terrain, and solar azimuth angle, respectively. This illumination parameter is the basis of the cosine correction formula, which is provided in Equation (8) of Table 3. The cosine correction only includes direct solar irradiance on the ground and ignores diffuse irradiance from the sky and adjacent terrain-reflected irradiance (Teillet, Guindon, and Goodenough 1982). However, the standard cosine correction is subject to overcorrection, which is most pronounced in low-illuminatedion areas (Moran et al. 1992; Soenen et al. 2008; Richter, Kellenberger, and Kaufmann 2009). The third implemented method is the pixel-based Minnaert correction (PBM), which accounts for non-Lambertian reflectance behaviour by means of an empirical Minnaert constant k. A global k-value was assessed for the entire image with Equation (9) in Table 3, assuming a homogeneous anisotropic nature of reflectance over the study area (Colby and Keating 1998; Gitas and Devereux 2006). More sophisticated approaches assessed wavelength-dependent k-values (Bishop and Colby 2002; Bishop, Shroder, and Colby 2003; Lu et al. 2008). The fourth implemented method, pixel-based C-correction (PBC), consisted of the topographic part of the integrated radiometric correction applied in the analysis of Kobayashi and Sanga-Ngoie (2008). The PBC method adds an additional factor C_λ to the cosine correction in Equation (10) of Table 3 to account for diffuse sky irradiance. The factor C_λ is the quotient of the intercept (b_λ) and the slope (m_λ) of the regression line. This additional

factor is function of terrain slope, solar zenith angle, topographic parameters derived from the SRTM (β and h-factor), and empirical parameters derived from the regression line between reflectance and cos β (C_λ and h_0-factor).

3.3. Integrated corrections

Many so-called 'integrated or combined correction methods' are presented and/or evaluated that consist of an atmospheric and a topographic component. For example, problems of overcorrection in the cosine correction are solved by the Hay's model (Hay 1979). This model implements TFs and the inclination and orientation of the surface account for the anisotropic distribution of the diffuse irradiance (Richter 1997; Guanter, Gomez-Chova, and Moreno 2008). Moreover, the so-called ATCOR3 correction integrates a MODTRAN atmospheric radiative transfer code and a modified Minnaert topographic method. This correction is similar to the combination of TF with PBM correction, although the atmospheric part of ATCOR3 implements MODTRAN, and the k-value is calculated differently. For reasons of comparison and visualization, ATCOR3 results are shown in parentheses within the TF and PBM combination in all the tables. The atmospheric part consists of an interactive and an automatic part (Richter 1996). In the interactive part, sensor type and relevant acquisition information were chosen, such as solar zenith angle, calibration information, and date. Second, a reference target (dense dark vegetation or water) was defined. The automatic phase calculated the visibility of the reference areas for the selected atmospheric characteristics and linked these characteristics with results obtained from the MODTRAN atmospheric radiative transfer code (Balthazar, Vanacker, and Lambin 2012). Preset ATCOR look-up tables were implemented to calculate the radiation components, as well as molecular and particulate absorption and scattering (Frey and Parlow 2009). The topographic ATCOR3 part is a modified Minnaert model based on a set of empirical rules (Richter, Kellenberger, and Kaufmann 2009). The normalized reflectance $\rho_{H,\lambda}$ is calculated with the correction factor $(\cos \beta/\cos \beta_T)^b$ in Equation (12), where b is a function of wavelength and vegetation cover, and β_T is a threshold value depending on θ_s:

$$\rho_{H,\lambda} = \rho_{T,\lambda}\left(\frac{\cos \beta}{\cos \beta_T}\right)^b \tag{12}$$

with b = 1/2 for non-vegetation; b = 3/4 for vegetation in the visible spectrum (λ < 720 nm); and b = 1/3 for vegetation if $\lambda \geq 720$ nm. The ATCOR3 method combines two empirical parameters to calculate the BRDF model: a lower boundary threshold of the correction factor and a threshold angle β_T (0–90°). The first parameter regulates the intensity of the correction by adapting the correction factor. If the correction factor is smaller than 0.25, it will be reset to 0.25 to prevent too strong a reduction (Richter and Schläpfer 2011). The second parameter is the threshold value of the incident solar angle, below which the Lambertian correction is applied. Above this threshold, the correction factor is applied to correct $\rho_{T,\lambda}$. This threshold was calculated based on θ_s plus an increment that depends on its initial value, as described in Equations (13)–(15) (Richter, Kellenberger, and Kaufmann 2009):

$$\beta_T = \theta_s + 20^\circ \text{ if } \theta_s \leq 45^\circ, \tag{13}$$

$$\beta_T = \theta_s + 15^\circ \text{ if } 45^\circ < \theta_s < 55^\circ, \tag{14}$$

$$\beta_T = \theta_s + 10^\circ \text{ if } \theta_s \geq 55^\circ \tag{15}$$

3.4. Evaluation of combined corrections

The combined correction methods were evaluated based on four analyses that test the homogeneity of reflectance values within a given land-cover class or within the entire image. Since forest was the dominant land-cover class, most statistical analyses were carried out on a set of 4000 forest pixels. These pixels were delineated on the basis of ground control points collected during field visits in May 2010 and July 2011 and visual interpretation of high-resolution satellite imagery (WorldView-2, eight bands, 46 cm resolution, acquisition date 13 October 2010). Forest pixels were classified into two groups, based on visual inspection of the satellite data and the value of cos β: illuminated (cos $\beta > 0.8$) and shaded forest pixels (cos $\beta < 0.6$). Visual inspection was performed by comparing the illuminated (sun-oriented) and shaded land units on true colour composites before and after correction.

The combined correction methods were evaluated based on the following four analyses.

(1) By comparing differences in reflectance values between shaded and illuminated slope groups, whereby each group was represented by 2000 forest pixels. These differences are expected to decrease after successful correction. Furthermore, the reflectance values between all pairs of shaded and illuminated slope groups before and after correction were tested with a dependent t-test for paired samples. Equation (16) was implemented where $\overline{z}$ is the difference in average reflectance values for shaded and illuminated slope groups, s is the sample standard deviation (SD), and n is the sample size (i.e. the 15 combined corrections and ATCOR3). The t-test was performed at the significance level 0.05.

$$t = \frac{\overline{z}}{s}\sqrt{n}. \tag{16}$$

(2) By calculating the coefficient of variation (CV) of reflectance values within the selected forest pixels with Equation (17). The CV is expected to decrease after a successful combined correction.

$$\text{CV} = 100\frac{\text{SD}}{\text{mean}}, \tag{17}$$

where SD is the standard deviation of the reflectance values within the forest class. To allow for a better interpretation, average CV values over all bands and $\text{CV}_{\text{difference}}$ values were calculated ($(\text{CV})_{\text{difference}} = (\text{CV})_{\text{before correction}} - (\text{CV})_{\text{after correction}}$).

(3) By examining the correlation between reflectance values and cos β before and after correction on a stratified sample of 5000 points over the entire image and on the selected forest pixels. This statistic was evaluated based on the regression slope and the p-value for testing the hypothesis of no correlation before and after

correction. The correlation is expected to decrease after a successful correction and correlations are significant if p-values are less than the significance level 0.05.

(4) By evaluating the mean normalized difference vegetation index ($NDVI_{difference}$), $(NDVI)_{before\ correction} - (NDVI)_{after\ correction}$, in the 4000 forest pixels for 15 combined corrections and ATCOR3. Furthermore, the reflectance values of all forest pixels were tested with the dependent t-test for paired samples (Equation (16)). This final analysis aimed at an improved evaluation of the impact of AC and TC methods.

4. Results

All analyses were performed on the 15 combined methods and ATCOR3. The tables show results for all combinations. In contrast, it was impractical to show all combinations in the figures. Therefore, six representative combinations were presented: (1) no AC and no TC; (2) DOS without TC; (3) DOS with band ratio; (4) TF with cosine; (5) TF with PBM; and (6) TF with PBC. These six combinations were selected, since all single AC and TC methods were included and represented the range of modelling complexity. Furthermore, these combinations represented the minimum, intermediate, and maximum results, and ATCOR3 results were similar to TF with PBM results.

4.1. *Differences in reflectances (shaded versus illuminated)*

Figure 2 shows reflectance values on illuminated (squares) and shaded slopes (circles) of the six bands and representative combinations for the selected forest pixels. In bands 1–3 of Figure 2(*a*), small differences were present between average uncorrected reflectance values of illuminated and shaded areas. In contrast, average reflectance values were less homogeneous in bands 4, 5, and 7. Combination of DOS without TC diminished differences between reflectance values of shaded and illuminated slopes (Figure 2(*b*)). Similar outputs were obtained for TF without TC. The application of DOS with band ratio overcorrected average reflectance values of visual bands, and the difference in average reflectance values was reduced in bands 4 to 7 (Figure 2(*c*)). After cosine with TF correction (Figure 2(*d*)), average reflectance values of shaded slopes were higher than illuminated slopes for bands 1 to 3, which indicated an overcompensation of reflectance values of shaded slopes. ATCOR3 and the TF with PBM combination showed a reduction of differences between average illuminated and shaded reflectances in all bands (Figure 2(*e*)). Implementation of TF with PBC correction performed best (Figure 2(*f*)), since average reflectance values of illuminated and shaded areas were similar.

The largest differences in reflectance values between illuminated and shaded forest slopes were observed in band 4. Table 4 shows that TCs had a stronger impact on the reflectance values than AC in this band. Differences after TC without AC ranged between −1.91% and 5.56%, while differences after only AC ranged between 8.54% and 9.86%. Furthermore, a combination of AC and TC methods resulted in the smallest differences with a minimum of −0.83% (TF with PBC) and a maximum of 5.83% (TF with band ratio). Results of the TF with PBM method (4.14%) were comparable to the results of ATCOR3 (3.73%). The smallest differences were found after TF with PBC correction (−0.83%). When the t-test was significant, an asterisk was added in Table 4. Significant results were present for the ATCOR3 method and for combined corrections with a PBM

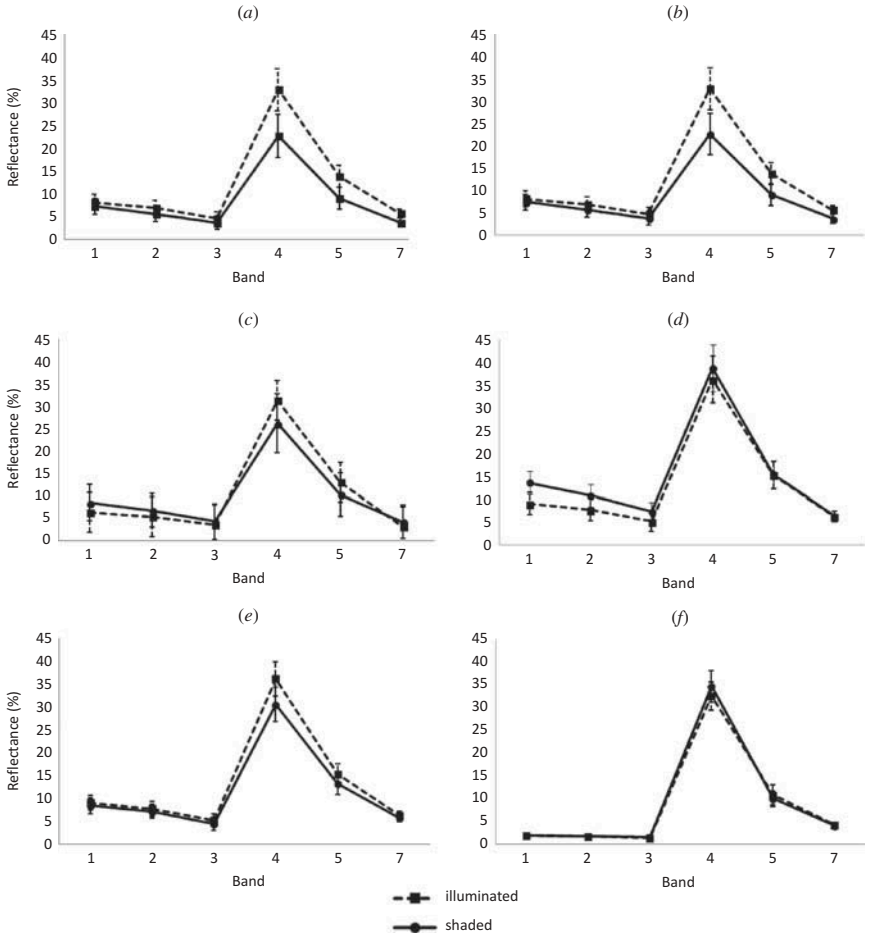

Figure 2. Average reflectance (%) calculated in the forest class as a function of spectral band: (*a*) no AC or TC; (*b*) DOS without TC; (*c*) DOS with band ratio; (*d*) TF with cosine; (*e*) TF with PBM; and (*f*) TF with PBC. The dashed line with square dots denotes the illuminated areas, the solid line with round dots denotes the shaded areas. The whiskers represent the SDs.

Table 4. Difference in average reflectance values (%) between illuminated and shaded forest slopes of band 4 for the 15 combined corrections and ATCOR3 (in parentheses). *Indicates a significant *t*-test between all pairs of shaded and illuminated slope groups before and after correction at the significance level 0.05.

	No TC	Band ratio	Cosine	PBM	PBC
No AC	10.16	5.56	−2.36	4.65	−1.91*
DOS	9.86	5.12	−2.34	5.04	−1.62*
TF	8.54	5.83	−1.56	4.14* (3.73*)	−0.83*

Table 5. CV values for each Thematic Mapper (TM) band, average CV and $CV_{difference}$ values over all bands (dimensionless) of the 15 combined corrections and ATCOR3 (in parentheses) for the selected forest pixels.

CV		TM 1	TM 2	TM 3	TM 4	TM 5	TM 7	Average	Difference
No AC	No TC	45.66	54.16	71.46	33.58	41.21	40.98	47.84	—
	Band ratio	42.44	57.74	75.51	30.32	45.49	42.08	48.93	1.09
	Cosine	44.68	54.32	67.82	24.81	40.97	39.05	45.27	2.57
	PBM	41.55	48.73	64.37	30.55	36.98	36.96	43.19	4.65
	PBC	41.51	46.56	62.71	30.14	35.09	37.60	42.27	5.57
DOS	No TC	44.93	53.60	67.18	34.90	40.78	39.40	46.80	1.04
	Band ratio	41.71	51.68	65.84	31.03	37.31	37.83	44.23	3.61
	Cosine	43.69	52.57	67.76	30.79	37.98	38.00	45.13	2.71
	PBM	41.28	49.53	63.86	27.77	36.98	37.40	42.80	5.04
	PBC	40.62	49.80	60.66	26.62	34.82	37.13	41.61	6.23
TF	No TC	43.80	52.85	65.86	33.18	40.26	39.98	45.99	1.85
	Band ratio	41.16	49.87	64.87	30.26	37.62	38.41	43.70	4.14
	Cosine	41.02	50.28	67.92	27.53	36.81	36.44	43.33	4.51
	PBM	40.05	46.58	63.53	23.45	33.55	30.84	39.67	8.17
		(39.74)	(46.89)	(62.87)	(23.16)	(33.87)	(29.61)	(39.36)	(8.48)
	PBC	39.26	46.50	61.58	24.39	34.80	28.91	39.24	8.60

or a PBC TC. The PBM method was only significant in combination with the transmittance-based AC. In contrast, the PBC correction was significant in combination with all ACs.

4.2. *Coefficient of variation*

Table 5 shows CV values for the selected forest pixels of each spectral band. Furthermore, average CV and $CV_{difference}$ values over all bands are presented. There was an increase in CV for bands 2, 3, and 5 only after band ratio without AC. All other combined corrections decreased the CV values. Results after TC without AC emphasized the effectiveness of TCs. The $CV_{difference}$ value after implementation of band ratio without AC was low (1.09). Furthermore, $CV_{difference}$ values increased after implementation of the three other TCs without AC. The $CV_{difference}$ value was highest for PBC (5.57), followed by PBM (4.65), and cosine (2.57), respectively. Table 5 also shows the performance of the two AC methods without TC. TF correction resulted in higher homogeneity than DOS correction, since the $CV_{difference}$ value after TF (1.85) was higher than the value after DOS (1.04). Best results were obtained after combined corrections. The combination of TF with PBC correction resulted in the highest homogeneity ($CV_{difference}$ of 8.60), closely followed by ATCOR3 ($CV_{difference}$ of 8.48) and TF with PBM correction ($CV_{difference}$ of 8.17).

4.3. *Correlation analysis*

A correlation between cos β and reflectance values before and after correction was performed on the selected forest pixels and the stratified sampling over the entire image. Tables 6 and 7 show results of both sampling strategies for all combined corrections in band 4. This band was selected based on the large differences in average reflectance values between illuminated and shaded slopes in the first statistical analysis. Before correction, correlation between cos β and reflectance values of both sampling

Table 6. Slopes and p-values of correlation analysis of the selected forest pixels in band 4 for the 15 combined corrections and ATCOR3 (in parentheses).

	No TC		Band ratio		Cosine		PBM		PBC	
	Slope	p	Slope	p	Slope	p	Slope	p	Slope	p
No AC	16.3	<0.001	−3.6	<0.001	−10.7	<0.001	3.0	0.312	2.9	0.326
DOS	13.9	<0.001	−3.3	<0.001	−9.8	<0.001	2.5	0.351	2.5	0.355
TF	12.5	<0.001	−3.0	<0.001	−9.4	<0.001	2.2 (2.1)	0.378 (0.386)	2.3	0.384

Table 7. Slopes and p-values of correlation analysis of the stratified sample in band 4 over the entire image for the 15 combined corrections and ATCOR3 (in parentheses).

	No TC		Band ratio		Cosine		PBM		PBC	
	Slope	p	Slope	p	Slope	p	Slope	p	Slope	p
No AC	14.6	<0.001	−2.5	<0.001	−9.3	<0.001	2.1	0.365	2.3	0.386
DOS	12.6	<0.001	−2.1	0.001	−8.5	<0.001	1.8	0.403	1.6	0.412
TF	11.4	<0.001	−1.9	0.001	−8.7	<0.001	1.3 (1.1)	0.465 (0.474)	0.7	0.483

strategies was positive. This is shown in Tables 6 and 7 by slope values of 16.3 and 14.6 respectively, and significance levels less than 0.05. The dependency of reflectance values on terrain illumination was reduced after correction. All tested corrections decreased slope values of the regression line, although correlations remained significant for some combinations. After combining DOS without TC, positive correlation was still present. Slope values had decreased from 16.3 to 13.9 and from 14.6 to 12.6, respectively. A significant correlation was still present for both samplings after combination of an AC with band ratio or cosine correction. In Tables 6 and 7, p-values were lower than the significance level, and slope values were negative. Implementation of DOS with band ratio and TF with cosine presented negative slope values in both tables. Combination of PBM or PBC without an AC resulted in a small dependency, with slope values smaller than 3.0 and p-values between 0.31 and 0.39. Dependency of reflectance values on terrain illumination was reduced after implementation of an AC with PBM or PBC method. For the forest pixels (Table 6), slope values ranged between 2.2 and 2.5, and p-values indicated that data were uncorrelated ($p > 0.05$). Table 7 shows that sampling over the entire image was even performing better than the forest sample, with slope values approximating 0 and p-values larger than 0.05. Results were improved most after ATCOR3 and combination of TF with PBM and PBC correction. Reflectance values and cos β were uncorrelated with reduced slope values of 1.1, 1.3, and 0.7, respectively.

Figure 3 shows true colour composite images before and after implementation of the six representative combined corrections. These images provide a better understanding of the study area and depict the removal of shading effects after combined correction. The image shows a 120 km^2 representative zoom of the study area as indicated in Figure 1. Without any corrections applied, there are clear differences between sun-oriented and opposite slopes in Figure 3(a). The output after DOS without a TC did not result in visual differences in Figure 3(b). A comparable output was obtained for TF without TC. In contrast, combined AC and TC methods changed the appearance of the images. Band

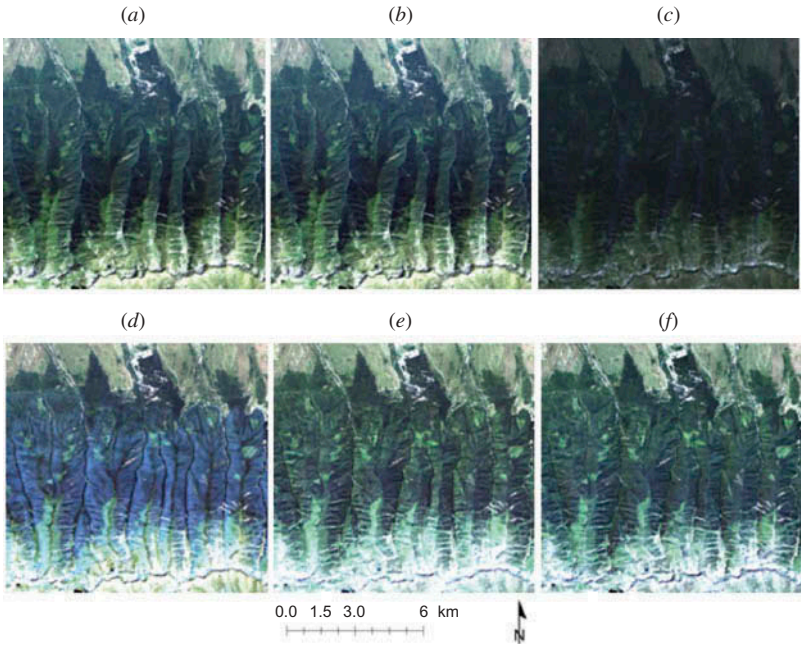

Figure 3. True colour composite images (RGB: bands 3, 2, and 1) of the zoom in the study area with a linear stretching: (*a*) no AC or TC; (*b*) DOS without TC; (*c*) DOS with band ratio; (*d*) TF with cosine; (*e*) TF with PBM; and (*f*) TF with PBC.

ratioing resulted in an overall lowering of reflectance values as expected after implementation of Equation (7) (Figure 3(*c*)). Combined TF and cosine correction resulted in a reduction of shades on poorly illuminated areas in Figure 3(*d*), although an overcorrection in the visible bands appeared. Best results were obtained after combination of TF with PBM or PBC correction in Figures 3(*e*) and (*f*). Differential illumination effects were reduced and spectral characteristics of sun-orientated and opposite slopes were similar.

4.4. $NDVI_{difference}$ value

Table 8 shows absolute values of mean $NDVI_{difference}$ in the selected forest pixels for all 15 combined corrections. Furthermore, a *t*-test was performed at the significance level 0.05. The absolute $NDVI_{difference}$ values are generally small and range between 0.0023 (no AC-band ratio) and 0.095 (TF-PBC; Table 8). Furthermore, the absolute $NDVI_{difference}$ values of AC methods without TC (0.042 and 0.049, respectively) are larger than TC

Table 8. Absolute values of mean $NDVI_{difference}$ (dimensionless) in the 4000 forest pixels for 15 combined corrections and ATCOR3 (in parentheses). *Indicates a significant *t*-test at the significance level 0.05.

	No TC	Band ratio	Cosine	PBM	PBC
No AC	—	0.023	0.028	0.033	0.032
DOS	0.042	0.065*	0.066*	0.069*	0.071*
TF	0.049*	0.068*	0.072*	0.094* (0.093*)	0.095*

methods without AC (respectively, 0.023, 0.028, 0.033, and 0.032). Compared to Table 4, more combinations are significant at the significance level 0.05. Especially more AC methods are significant, which indicates that the AC methods have more influence in the red and near-infrared bands (respectively, TM 3 and 4).

5. Discussion

This analysis provided new insights for 15 permutations of two atmospheric and/or four TCs along with uncorrected imagery. Generally, visible bands presented small differences between average reflectance values of illuminated and shaded areas. These differences were produced by larger atmospheric than topographic distortions in bands 1 to 3 due to scattering and diffusion, and confirmed by results of previous research (Kobayashi and Sanga-Ngoie 2008; Schroeder et al. 2006; Vicente-Serrano, Perezcabello, and Lasanta 2008). Implementation of TF with cosine indicated an overcorrection of reflectance values of shaded slopes. The overcorrection of areas under low illumination conditions – especially steep terrain where incident angles approach 90° – has been found in several analyses (Hantson and Chuvieco 2011; Meyer et al. 1993; Teillet, Guindon, and Goodenough 1982). ATCOR3 and combination of TF with PBM and PBC showed a reduction of differences between average reflectance values in all bands and significant *t*-test results. These results were comparable to experiments conducted by Huang et al. (2008), Wen et al. (2009), and Vicente-Serrano et al. (2008). In our analysis, average $CV_{difference}$ values increased after implementation of advanced TCs without AC. The average $CV_{difference}$ value was highest for PBC, followed by PBM and cosine. Correlation analysis showed that PBM or PBC without an AC resulted in a small dependency. However, this dependency was even reduced after combined correction. This proved that TC methods had a larger impact on the results than AC methods. Valid explanations were the application of only one Landsat footprint and the mountainous terrain. Dependency between cos β and reflectance values was decreased most after ATCOR3 and the combination of TF with PBM or PBC. Similar results were obtained in a previous analysis by Kobayashi and Sanga-Ngoie (2008). The largest illumination effects were observed in the forest class, which explained an improved performance of sampling over the entire Landsat image.

Considering the overall results, this analysis showed that most complex combined corrections were most accurate but also most difficult to automate. Furthermore, the added value of complex TC methods was high, while the added value of AC methods was limited. These results confirmed the findings of previous analyses by Eiumnoh and Shrestha (2000) and Hale and Rock (2003), where topographic effects had a larger impact on reflectance values than atmospheric effects. Therefore, an additional *t*-test was performed on $NDVI_{difference}$ values of the selected forest pixels. This analysis showed that the difference values of AC methods were higher and that the AC methods had a higher influence on the significance results. This is explained by a larger influence of AC methods on the red and near-infrared channels (respectively, band 3 and 4), while TC methods are more spectrally invariant in these two bands, although AC methods are normally expected to increase the contrast between different land-cover types. Therefore, the AC methods were included since these methods are essential for vegetation indices and time-series analyses. However, in this article, the four analyses that test the homogeneity of reflectance values were performed in only one class (forest) and on a single Landsat image. Consequently, in one class and image, a higher homogeneity of reflectance values and less scatter is expected. In general, application of a combined correction

based on a complex TC component and a rather straightforward AC component was justified in this case study.

6. Conclusions

In this analysis, the performance of the combination of three atmospheric and five TCs and the integrated ATCOR3 method was evaluated along with uncorrected Landsat imagery. The most similar studies to date missed a thorough comparison between different AC and TC methods, while this analysis decomposed integrated models in an AC and a TC component and systematically evaluated the effects of all combinations. A statistical comparison of illuminated *versus* shaded reflectance values without any correction indicated that major differences were present in bands 4 to 7. After implementation of combined corrections, these differences were reduced. The smallest differences in reflectance values were present after ATCOR3 correction or combination of an AC with PBM or PBC. Furthermore, most of these combined corrections resulted in significant *t*-test results. Comparable conclusions were drawn from the analysis of the coefficients of variation for the forest sampling. The CV of each spectral band decreased after a combined correction. Overall results indicated that TC had a larger impact on the reflectance values than AC. The added value of AC methods on reflectance values was relatively low, since only one forest class, a single Landsat image and specific evaluation methods were implemented. However, the NDVI analysis indicated that AC methods resulted in a larger impact on the spectral information in bands 3 and 4. Therefore, results of the AC methods were included since these methods are essential for vegetation indices and time-series analyses. In this study, ATCOR3 and combinations of TF with PBM or PBC performed best, although these methods required the largest amount of input data.

The added value of this study was the decomposition of integrated models and the systematic evaluation along with uncorrected imagery. This case study proved that the benefits in reduction of atmospheric and topographic distortions justified automation of more complex corrections in mountain areas.

Acknowledgements

This research was conducted for the project ‘Remote sensing of the forest transition and its ecosystem impacts in mountain environments’ (FOMO). The authors would like to thank Rudolf Richter and Daniel Schlaepfer for their help with this article.

Funding

The work was supported by the Research Programme for Earth Observation Stereo II of the Belgian Science Policy (BELSPO) [contract SR/00/133].

References

Balthazar, V., V. Vanacker, and E. Lambin. 2012. “Evaluation and Parameterization of ATCOR3 Topographic Correction Method for Forest Cover Mapping in Mountain Areas.” *International Journal of Applied Earth Observation and Geoinformation* 18: 436–450. doi:10.1016/j.jag.2012.03.010.

Berk, A., L. S. Bernstein, G. P. Anderson, D. C. Robertson, J. H. Chetwynd, S. M. Adler-Golden, and S. M. Adler-Golden. 1998. “MODTRAN Cloud and Multiple Scattering Upgrades with Application to AVIRIS.” *Remote Sensing of Environment* 65: 367–375. doi:10.1016/S0034-4257(98)00045-5.

Bird, R. E., and C. Riordan. 1986. "Simple Solar Spectral Model for Direct and Diffuse Irradiance on Horizontal and Tilted Planes at the Earth's Surface for Cloudless Atmospheres." *Journal of Climate and Applied Meteorology* 25: 87–97. doi:2.0.CO;2",1,0,0>10.1175/1520-0450(1986)025<0087:SSSMFD>2.0.CO;2.

Bishop, M. P., and J. D. Colby. 2002. "Anisotropic Reflectance Correction of SPOT-3 HRV Imagery." *International Journal of Remote Sensing* 23: 2125–2131. doi:10.1080/01431160110097231.

Bishop, M. P., J. F. Shroder, and J. D. Colby. 2003. "Remote Sensing and Geomorphometry for Studying Relief Production in High Mountains." *Geomorphology* 55: 345–361. doi:10.1016/S0169-555X(03)00149-1.

Bruce, C. M., and D. W. Hilbert. 2004. *Pre-Processing Methodology for Application to Landsat TM/ETM+ Imagery of the Wet Tropics*. Research Report. Cairns: Cooperative Research Centre for Tropical Rainforest Ecology and Management. Accessed July 13, 2013. http://www.rrrc.org.au/rfcrc/downloads/44_landsat_preprocessing.pdf

Chander, G., B. L. Markham, and D. L. Helder. 2009. "Summary of Current Radiometric Calibration Coefficients for Landsat MSS, TM, ETM+, and EO-1 ALI Sensors." *Remote Sensing of Environment* 113: 893–903. doi:10.1016/j.rse.2009.01.007.

Chavez, P. S. 1996. "Image-Based Atmospheric Correction-Revisited and Improved." *Photogrammetric Engineering and Remote Sensing* 62: 1025–1036.

Civco, D. L. 1989. "Topographic Normalization of Landsat Thematic Mapper Digital Imagery." *Photogrammetric Engineering and Remote Sensing* 55: 1303–1309.

Colby, J. D. 1991. "Topographic Normalization in Rugged Terrain." *Photogrammetric Engineering and Remote Sensing* 57: 531–537.

Colby, J. D., and P. L. Keating. 1998. "Land Cover Classification using Landsat TM Imagery in the Tropical Highlands: The Influence of Anisotropic Reflectance." *International Journal of Remote Sensing* 19: 1479–1500. doi:10.1080/014311698215306.

Conese, C., M. A. Gilabert, F. Maselli, and L. Bottai. 1993. "Topographic Normalization of TM Scenes through the Use of an Atmospheric Correction Method and Digital Terrain Models." *Photogrammetric Engineering and Remote Sensing* 59: 1745–1753.

Cuo, L., J. B. Vogler, and J. M. Fox. 2010. "Topographic Normalization for Improving Vegetation Classification in a Mountainous Watershed in Northern Thailand." *International Journal of Remote Sensing* 31: 3037–3050. doi:10.1080/01431160903154333.

Defries, R. S., J. A. Foley, and G. P. Asner. 2004. "Land-Use Choices: Balancing Human Needs and Ecosystem Function." *Frontiers in Ecology and the Environment* 2: 249–257. doi:10.1890/1540-9295(2004)002[0249:LCBHNA]2.0.CO;2.

Eiumnoh, A., and R. P. Shrestha. 2000. "Application of DEM Data to Landsat Image Classification: Evaluation in Tropical Wet-Dry Climate." *Photogrammetric Engineering and Remote Sensing* 66: 297–304.

Ekstrand, S. 1996. "Landsat TM-Based Forest Damage Assessment: Correction for Topographic Effects." *Photogrammetric Engineering and Remote Sensing* 62: 151–161.

Foley, J. A., R. Defries, G. P. Asner, C. Barford, G. Bonan, S. R. Carpenter, F. S. Chapin, M. T. Coe, G. C. Daily, H. K. Gibbs, J. H. Helkowski, T. Holloway, E. A. Howard, C. J. Kucharik, C. Monfreda, J. A. Patz, I. C. Prentice, N. Ramankutty, and P. K. Snyder. 2005. "Global Consequences of Land Use." *Science* 309: 570–574. doi:10.1126/science.1111772.

Frey, C., and E. Parlow. 2009. "Geometry Effect on the Estimation of Band Reflectance in an Urban Area." *Theoretical and Applied Climatology* 96: 395–406. doi:10.1007/s00704-008-0048-y.

Gao, Y., and W. Zhang. 2009. "A Simple Empirical Topographic Correction Method for ETM+ Imagery." *International Journal of Remote Sensing* 30: 2259–2275. doi:10.1080/01431160802549336.

Gilabert, M. A., C. Conese, and F. Maselli. 1994. "An Atmospheric Correction Method for the Automatic Retrieval of Surface Reflectances from TM Images." *International Journal of Remote Sensing* 15: 2065–2086. doi:10.1080/01431169408954228.

Giovanni Portal. 2012. *Interactive Visualization and Analysis*. Washington, DC: Goddard Earth Sciences, Data and Information Services Center. Accessed July 16, 2013. http://disc.sci.gsfc.nasa.gov/giovanni/overview/index.html

Gitas, I. Z., and B. J. Devereux. 2006. "The Role of Topographic Correction in Mapping Recently Burned Mediterranean Forest Areas from Landsat TM Images." *International Journal of Remote Sensing* 27: 41–54. doi:10.1080/01431160500182992.

Gu, D., and A. Gillespie. 1998. "Topographic Normalization of Landsat TM Images of Forest Based on Subpixel Sun-Canopy-Sensor Geometry." *Remote Sensing of Environment* 64: 166–175. doi:10.1016/S0034-4257(97)00177-6.

Guanter, L., L. Gomez-Chova, and J. Moreno. 2008. "Coupled Retrieval of Aerosol Optical Thickness, Columnar Water Vapor and Surface Reflectance Maps from ENVISAT/MERIS Data over Land." *Remote Sensing of Environment* 112: 2898–2913.

Hale, S. R., and B. N. Rock. 2003. "Impact of Topographic Normalization on Land-Cover Classification Accuracy." *Photogrammetric Engineering and Remote Sensing* 69: 785–791. doi:10.14358/PERS.69.7.785.

Hantson, S., and E. Chuvieco. 2011. "Evaluation of Different Topographic Correction Methods for Landsat Imagery." *International Journal of Applied Earth Observation and Geoinformation* 13: 691–700. doi:10.1016/j.jag.2011.05.001.

Hay, J. E. 1979. "Calculation of Monthly Mean Solar Radiation for Horizontal and Inclined Surfaces." *Solar Energy* 23: 301–307. doi:10.1016/0038-092X(79)90123-3.

Hirt, C., M. S. Filmer, and W. E. Featherstone. 2010. "Comparison and Validation of the Recent Freely-Available ASTER GDEM Ver1, SRTM Ver4.1 and GEODATA DEM-9S Ver3 Digital Elevation Models over Australia." *Australian Journal of Earth Sciences* 57: 337–347. doi:10.1080/08120091003677553.

Huang, H., P. Gong, N. Clinton, and F. Hui. 2008. "Reduction of Atmospheric and Topographic Effect on Landsat TM Data for Forest Classification." *International Journal of Remote Sensing* 29: 5623–5642. doi:10.1080/01431160802082148.

Jensen, J. R. 1996. *Introduction Digital Image Processing: A Remote Sensing Perspective*, 526 p. Englewood Cliffs, NJ: Prentice-Hall.

Johnson, R. L., D. R. Peddle, and R. J. Hall. 2000. A Modelled-Based Sub-Pixel Scale Mountain Terrain Normalization Algorithm for Improved LAI Estimation from Airborne Casi Imagery. In *Proceedings 22nd Canadian Symposium on Remote Sensing*, Victoria, BC, August 21–25, 415–424. Ottawa, ON: Canadian Aeronautics and Space Institute.

Kneizys, F. X., E. P. Shettle, L. W. Abreu, J. H. Chetwynd, G. P. Anderson, W. O. Gallery, J. E. A. Selby, and S. A. Clough. 1988. *User's Guide to LOWTRAN-7*, 146 p. Bedford, MA: Air Force Geophysics Laboratory, Hanscom.

Kobayashi, S., and K. Sanga-Ngoie. 2008. "The Integrated Radiometric Correction of Optical Remote Sensing Imageries." *International Journal of Remote Sensing* 29: 5957–5985. doi:10.1080/01431160701881889.

Kuemmerle, T., D. Müller, P. Griffiths, and M. Rusu. 2009. "Land Use Change in Southern Romania after the Collapse of Socialism." *Regional Environmental Change* 9: 1–12. doi:10.1007/s10113-008-0050-z.

Lambin, E. F., and H. J. Geist. 2006. *Land Use and Land Cover Change, Local Processes and Global Impacts*, 236 p. Berlin: Springer-Verlag.

Lambin, E. F., and P. Meyfroidt. 2010. "Land Use Transitions: Socio-Ecological Feedback versus Socio-Economic Change." *Land Use Policy* 27: 108–118. doi:10.1016/j.landusepol.2009.09.003.

Leica Geosystems. 2006. "Imagine Autosync." White Paper, Leice Geosystems Geospatial Imaging, Norcross, GA. Accessed June 25, 2013. http://geospatial.intergrapgh.com/products/ERDASIMAGINE/IMAGINEAutoSync/Details.aspx

Lenot, X., V. Achard, and L. Poutier. 2009. "SIERRA: A New Approach to Atmospheric and Topographic Corrections for Hyperspectral Imagery." *Remote Sensing of Environment* 113: 1664–1677. doi:10.1016/j.rse.2009.03.016.

Liang, S., and H. Fang. 2004. "An Improved Atmospheric Correction Algorithm for Hyperspectral Remotely Sensed Imagery." *IEEE Geoscience and Remote Sensing Letters* 1: 112–117. doi:10.1109/LGRS.2004.824747.

Liang, S., H. Fang, and M. Chen. 2001. "Atmospheric Correction of Landsat ETM+ Land Surface Imagery. I. Methods." *IEEE Transactions on Geoscience and Remote Sensing* 39: 2490–2498. doi:10.1109/36.964986.

Lu, D., H. Ge, S. He, A. Xu, G. Zhou, and H. Du. 2008. "Pixel-based Minnaert Correction Method for Reducing Topographic Effects on a Landsat-7 ETM+ Image." *Photogrammetric Engineering and Remote Sensing* 74: 1343–1350. doi:10.14358/PERS.74.11.1343.

Meyer, P., K. L. Itten, T. Kellenberger, S. Sandmeier, and R. Sandmeier. 1993. "Radiometric Corrections of Topographically Induced Effects on Landsat TM Data in an Alpine

Environment." *ISPRS Journal of Photogrammetry and Remote Sensing* 48: 17–28. doi:10.1016/0924-2716(93)90028-L.
Minnaert, N. 1941. "The Reciprocity Principle in Lunar Photometry." *The Astrophysical Journal* 93: 403–410. doi:10.1086/144279.
Mitri, G. H., and I. Z. Gitas. 2004. "A Performance Evaluation of a Burned Area Object-based Classification Model When Applied to Topographically and Non-Topographically Corrected TM Imagery." *International Journal of Remote Sensing* 25: 2863–2870. doi:10.1080/01431160410001688321.
Moran, M. S., R. D. Jackson, P. N. Slater, and P. M. Teillet. 1992. "Evaluation of Simplified Procedures for Retrieval of Land Surface Reflectance Factors from Satellite Sensor Output." *Remote Sensing of Environment* 41: 169–184. doi:10.1016/0034-4257(92)90076-V.
NIS Romania. 2010. *Database of Localities*. Bucharest: National Institute of Statistics.
Ono, A., K. Kajiwara, and Y. Honda. 2007. "Development of Vegetation Index Using Radiant Spectra Normalized by their Arithmetic Mean." Proceedings 42nd Conference of the Remote Sensing Society of Japan, Tokyo, Japan, May 10–11, 99–100.
Rabus, B., M. Eineder, A. Roth, and R. Bamler. 2003. "The Shuttle Radar Topography Mission—A New Class of Digital Elevation Models Acquired by Spaceborne Radar." *ISPRS Journal of Photogrammetry and Remote Sensing* 57: 241–262. doi:10.1016/S0924-2716(02)00124-7.
Rahman, H., and G. Dedieu. 1994. "SMAC: A Simplified Method for the Atmospheric Correction of Satellite Measurements in the Solar Spectrum." *International Journal of Remote Sensing* 15: 123–143. doi:10.1080/01431169408954055.
Riano, D., E. Chuvieco, F. J. Salas, and I. Aguado. 2003. "Assessment of Different Topographic Corrections in Landsat-TM Data for Mapping Vegetation Types." *IEEE Transactions on Geoscience and Remote Sensing* 41: 1056–1061. doi:10.1109/TGRS.2003.811693.
Richter, R. 1996. "Atmospheric Correction of Satellite Data with Haze Removal Including a Haze/Clear Transition Region." *Computers and Geosciences* 22: 675–681. doi:10.1016/0098-3004(96)00010-6.
Richter, R. 1997. "Correction of Atmospheric and Topographic Effects for High Spatial Resolution Satellite Imagery." *International Journal of Remote Sensing* 18: 1099–1111. doi:10.1080/014311697218593.
Richter, R. 1998. "Correction of Satellite Imagery over Mountainous Terrain." *Applied Optics* 37: 4004–4015. doi:10.1364/AO.37.004004.
Richter, R., T. Kellenberger, and H. Kaufmann. 2009. "Comparison of Topographic Correction Methods." *Remote Sensing* 1: 184–196. doi:10.3390/rs1030184.
Richter, R., and D. Schläpfer. 2002. "Geo-Atmospheric Processing of Airborne Imaging Spectrometry Data. Part 2: Atmospheric/Topographic Correction." *International Journal of Remote Sensing* 23: 2631–2649. doi:10.1080/01431160110115834.
Richter, R., and D. Schläpfer. 2011. *Atmospheric/Topographic Correction for Satellite Imagery. ATCOR 2/3 User Guide*. Version 8.2.0. BETA, February 2012, Wil. Accessed June 15, 2013. http://www.dlr.de/eoc/Portaldata/60/Resources/dokumente/5_tech_mod/atcor3_manual_2012.pdf.
Sandmeier, S., and K. I. Itten. 1997. "A Physically-based Model to Correct Atmospheric and Illumination Effects in Optical Satellite Data of Rugged Terrain." *IEEE Transactions on Geoscience and Remote Sensing* 35: 708–717. doi:10.1109/36.581991.
Schroeder, T. A., W. B. Cohen, C. Song, M. J. Canty, and Z. Yang. 2006. "Radiometric Correction of Multi-Temporal Landsat Data for Characterization of Early Successional Forest Patterns in Western Oregon." *Remote Sensing of Environment* 103: 16–26. doi:10.1016/j.rse.2006.03.008.
Singh, S., J. K. Sharma, and V. D. Mishra. 2011. "Comparison of Different Topographic Correction Methods Using Awifs Satellite Data." *International Journal of Advanced Engineering Sciences and Technologies* 7: 103–109.
Smith, G. M., and E. J. Milton. 1999. "The Use of the Empirical Line Method to Calibrate Remotely Sensed Data to Reflectance." *International Journal of Remote Sensing* 20: 2653–2662. doi:10.1080/014311699211994.
Smith, J. A., T. L. Lin, and K. J. Ranson. 1980. "The Lambertian Assumption and Landsat Data." *Photogrammetric Engineering and Remote Sensing* 46: 1183–1189.
Soenen, S. A., D. R. Peddle, C. A. Coburn, R. J. Hall, and F. G. Hall. 2008. "Improved Topographic Correction of Forest Image Data Using a 3-D Canopy Reflectance Model in Multiple Forward Mode." *International Journal of Remote Sensing* 29: 1007–1027. doi:10.1080/01431160701311291.

Song, C., C. E. Woodcock, K. C. Seto, M. P. Lenney, and S. A. Macomber. 2001. "Classification and Change Detection Using Landsat TM Data: When and How to Correct Atmospheric Effects." *Remote Sensing of Environment* 75: 230–244. doi:10.1016/S0034-4257(00)00169-3.

Sriwongsitanon, N., K. Surakit, and S. Thianpopirug. 2011. "Influence of Atmospheric Correction and Number of Sampling Points on the Accuracy of Water Clarity Assessment Using Remote Sensing Application." *Journal of Hydrology* 401: 203–220. doi:10.1016/j.jhydrol.2011.02.023.

Teillet, P. M., B. Guindon, and D. G. Goodenough. 1982. "On the Slope-Aspect Correction of Multispectral Scanner Data." *Canadian Journal of Remote Sensing* 8: 84−106.

Turner, B. L., E. F. Lambin, and A. Reenberg. 2007. "The Emergence of Land Change Science for Global Environmental Change and Sustainability." *Proceedings of the National Academy of Sciences of the United States of America* 104: 20666–20671. doi:10.1073/pnas.0704119104.

Van Ede, R. 2004. "Destriping and Geometric Correction of an ASTER Level 1A Image." Master thesis, Utrecht University, Utrecht, 36 p.

Veraverbeke, S., S. Lhermitte, W. W. Verstraeten, and R. Goossens. 2011. "A Time Integrated MODIS Burn Severity Assessment Using the Multi-Temporal Differenced Normalized Burn Ratio (Dnbrmt)." *International Journal of Applied Earth Observation and Geoinformation* 13: 52–58. doi:10.1016/j.jag.2010.06.006.

Vermote, E. F., N. Z. El Saleous, C. O. Justice, Y. J. Kaufman, J. Privette, L. Remer, J. C. Roger, and D. Tanré. 1997. "Atmospheric Correction of Visible to Middle-Infrared EOS-MODIS Data over Land Surfaces: Background, Operational Algorithm and Validation." *Journal of Geophysical Research* 102: 17131–17141. doi:10.1029/97JD00201.

Vicente-Serrano, S. M., F. Perezcabello, and T. Lasanta. 2008. "Assessment of Radiometric Correction Techniques in Analyzing Vegetation Variability and Change Using Time Series of Landsat Images." *Remote Sensing of Environment* 112: 3916–3934. doi:10.1016/j.rse.2008.06.011.

Vincini, M., and E. Frazzi. 2003. "Multitemporal Evaluation of Topographic Normalization Methods on Deciduous Forest TM Data." *IEEE Transactions on Geoscience and Remote Sensing* 41: 2586–2590. doi:10.1109/TGRS.2003.817416.

Wen, J., Q. Liu, Q. Liu, Q. Xiao, and X. Li. 2009. "Parametrized BRDF for Atmospheric and Topographic Correction and Albedo Estimation in Jiangxi Rugged Terrain, China." *International Journal of Remote Sensing* 30: 2875–2896. doi:10.1080/01431160802558618.

World Health Organization. 2005. *Ecosystems and Human Well-Being, Health Synthesis, Millennium Ecosystem Assessment*, 64 p. Geneva: WHO Press.

Wu, J., M. E. Bauer, D. Wang, and S. Manson. 2008. "A Comparison of Illumination Geometry-Based Methods for Topographic Correction of Quickbird Images of an Undulant Area." *ISPRS Journal of Photogrammetry and Remote Sensing* 63: 223–236. doi:10.1016/j.isprsjprs.2007.08.004.

Zhang, Z., R. R. De Wulf, F. M. B. Van Coillie, L. P. C. Verbeke, E. M. De Clercq, and X. Ou. 2011. "Influence of Different Topographic Correction Strategies on Mountain Vegetation Classification Accuracy in the Lancang Watershed, China." *Journal of Applied Remote Sensing* 5: 1–21.

Zhang, W., and Y. Gao. 2011. "Topographic Correction Algorithm for Remotely Sensed Data Accounting for Indirect Irradiance." *International Journal of Remote Sensing* 32: 1807–1824. doi:10.1080/01431161003623441.

Zhao, W., M. Tamura, and H. Takahashi. 2001. "Atmospheric and Spectral Corrections for Estimating Surface Albedo from Satellite Data Using 6S Code." *Remote Sensing of Environment* 76: 202–212. doi:10.1016/S0034-4257(00)00204-2.